01 Oct 2008

Adaptive Control of Freeze-Form Extrusion Fabrication Processes

Xiyue Zhao

Robert G. Landers
Missouri University of Science and Technology, landersr@mst.edu

Ming-Chuan Leu
Missouri University of Science and Technology, mleu@mst.edu

AFRL-RX-WP-TP-2008-4348

ADAPTIVE CONTROL OF FREEZE-FORM EXTRUSION FABRICATION PROCESSES (PREPRINT)

Xiyue Zhao, Robert G. Landers, and Ming C. Leu

University of Missouri-Rolla

MAY 2008

AIR FORCE RESEARCH LABORATORY
MATERIALS AND MANUFACTURING DIRECTORATE
WRIGHT-PATTERSON AIR FORCE BASE, OH 45433-7750
AIR FORCE MATERIEL COMMAND
UNITED STATES AIR FORCE

REPORT DOCUMENTATION PAGE

Form Approved
OMB No. 0704-0188

1. REPORT DATE *(DD-MM-YY)*	2. REPORT TYPE	3. DATES COVERED *(From - To)*
May 2008	Conference Paper Preprint	

4. TITLE AND SUBTITLE
ADAPTIVE CONTROL OF FREEZE-FORM EXTRUSION FABRICATION PROCESSES (PREPRINT)

5a. CONTRACT NUMBER
FA8650-04-C-5704

5b. GRANT NUMBER

5c. PROGRAM ELEMENT NUMBER
78011F

6. AUTHOR(S)
Xiyue Zhao, Robert G. Landers, and Ming C. Leu

5d. PROJECT NUMBER
2865

5e. TASK NUMBER
25

5f. WORK UNIT NUMBER
25100000

7. PERFORMING ORGANIZATION NAME(S) AND ADDRESS(ES)
University of Missouri-Rolla
1870 Miner Circle
Rolla, MO 65409-0970

8. PERFORMING ORGANIZATION REPORT NUMBER

9. SPONSORING/MONITORING AGENCY NAME(S) AND ADDRESS(ES)
Air Force Research Laboratory
Materials and Manufacturing Directorate
Wright-Patterson Air Force Base, OH 45433-7750
Air Force Materiel Command
United States Air Force

10. SPONSORING/MONITORING AGENCY ACRONYM(S)
AFRL/RXLMP

11. SPONSORING/MONITORING AGENCY REPORT NUMBER(S)
AFRL-RX-WP-TP-2008-4348

12. DISTRIBUTION/AVAILABILITY STATEMENT
Approved for public release; distribution unlimited.

13. SUPPLEMENTARY NOTES
Conference paper submitted to the proceedings of the 2008 ASME Dynamic Systems and Control Conference, Ann Arbor, MI. PAO Case Number: WPAFB 08-3372; Clearance Date: 22 May 2008. This work was funded in whole or in part by Department of the Air Force contract FA8650-04-C-5704. The U.S. Government has for itself and others acting on its behalf an unlimited, paid-up, nonexclusive, irrevocable worldwide license to use, modify, reproduce, release, perform, display, or disclose the work by or on behalf of the U.S. Government. Paper contains color.

14. ABSTRACT
Freeze-form Extrusion Fabrication (FEF) is an additive manufacturing process that extrudes high solids loading aqueous ceramic pastes in a layer-by-layer fashion below the paste freezing temperature for component fabrication. Due to effects such as the air bubble release, agglomerate breakdown, change in paste properties during extrusion as a result of liquid phase migration, etc., the extrusion force is difficult to control. In this paper, an adaptive controller is proposed to regulate the extrusion force. Recursive Least Squares is used to estimate extrusion force model parameters during fabrication and a low-order control scheme capable of tracking general reference trajectories is designed and implemented to regulate the extrusion process. The controller is implemented to regulate the extrusion process. The controller is implemented fro sinusoidal, triangular, and square reference trajectories and the results demonstrate excellent tracking performance of the adaptive extrusion force controller. Several parts were fabricated with the adaptive extrusion force controller. These results illustrate the need for extrusion force control and that variable reference extrusion.

15. SUBJECT TERMS
Ceramic Paste Extrusion, Solid Freeform Fabrication, Adaptive Extrusion Force Control

16. SECURITY CLASSIFICATION OF:			17. LIMITATION OF ABSTRACT:	18. NUMBER OF PAGES	19a. NAME OF RESPONSIBLE PERSON (Monitor)
a. REPORT	b. ABSTRACT	c. THIS PAGE			Todd J. Turner
Unclassified	Unclassified	Unclassified	SAR	46	19b. TELEPHONE NUMBER *(Include Area Code)* N/A

Standard Form 298 (Rev. 8-98)
Prescribed by ANSI Std. Z39-18

Adaptive Control of Freeze–form Extrusion Fabrication Processes

Xiyue Zhao, Robert G. Landers[1], and Ming C. Leu

Department of Mechanical and Aerospace Engineering

Missouri University of Science and Technology, Rolla, Missouri, 65401–0050

{xzd2c;landersr;mleu}@mst.edu

Abstract

Freeze–form Extrusion Fabrication (FEF) is an additive manufacturing process that extrudes high solids loading aqueous ceramic pastes in a layer–by–layer fashion below the paste freezing temperature for component fabrication. Due to effects such as the air bubble release, agglomerate breakdown, change in paste properties during extrusion as a result of liquid phase migration, etc., the extrusion force is difficult to control. In this paper, an adaptive controller is proposed to regulate the extrusion force. Recursive Least Squares is used to estimate extrusion force model parameters during fabrication and a low–order control scheme capable of tracking general reference trajectories is designed and implemented to regulate the extrusion process. The controller is implemented for sinusoidal, triangular, and square reference trajectories and the results demonstrate excellent tracking performance of the adaptive extrusion force controller. Several parts were fabricated with the adaptive extrusion force controller. These results illustrate the need for extrusion force control and that variable reference extrusion force profiles are required to fabricate complex features.

1 Corresponding Author

Keywords

Ceramic Paste Extrusion, Solid Freeform Fabrication, Adaptive Extrusion Force Control

Introduction

Solid Freeform Fabrication (SFF) has tremendous potential for becoming an efficient manufacturing technique for 3–D ceramic component fabrication since it is a tool–less fabrication process and, as compared to conventional fabrication techniques, does not require costly and time–consuming mold preparation. Most SFF techniques for ceramic component fabrication involve the use of organic binders. In some processes, such as the Fused Deposition of Ceramics process, the binder content may be as high as 40 to 50 vol. %. The organic binder must be removed during post processing. Binder removal is very time–consuming and generates harmful wastes that are undesirable for the environment [1].

Freeze–form Extrusion Fabrication (FEF) uses an aqueous ceramic paste with solids loading up to 50 vol. %; however, water is the main liquid medium and the organic binder content is only 2–4 vol. % [2]. In FEF, an aqueous–based ceramic paste is extruded using a ram extruder and deposited on a substrate. After each layer is deposited, the extrusion mechanism moves up one layer thickness and the next layer is deposited. When fabrication is complete, the part is freeze–dried to prevent crack formation. After freeze–drying, the binder is then removed in a rapid heating cycle because of the low binder content. Finally, the parts are sintered at a high temperature (e.g., 1550°*C* for alumina). Because the organic binder content is reduced to 2–4 vol. %, FEF is an environmentally friendly paste extrusion technique for ceramic part fabrication.

Most research studies in extrusion processes are concerned with screw–based polymer (melt) extrusion processes. In these processes, in–process measurement of viscosity and throughput (extrusion rate) is generally not available; therefore, most research studies have concentrated on indirect control of these variables via the regulation of melt temperature and pressure. Costin *et al*. [3] provided a review of the early dynamics and control work in this area, which focused on classical control techniques. Hassan and Parnaby [4] used optimization and off–line curve fitting of experimental data to define a quasi–linear steady–state model. A cascade controller, using one–step–ahead forecasts of melt temperature and melt pressure, calculated and changed the screw speed, barrel/die wall temperature, and restrictor valve angular position set points to maintain a desired extrusion rate. Costin *et al*. [5] used step tests to determine empirical models of melt temperature and pressure in a single screw extruder. Proportional plus integral and self tuning regulator controllers were implemented to remove the long–term drift in the pressure level and surging in the pressure caused by a change in polymer quality. More recently, Previdi *et al*. [6] determined empirical first–order models, with delays, from screw system input voltage to pressure and from seven heater regulator duty cycles to seven extruder temperatures. Separate digital proportional plus integral plus derivative controllers were implemented. The results showed the controllers were able to simultaneously regulate the pressure and temperatures at constant reference values. These linear techniques generally cannot capture the system's nonlinearities; therefore, they are only suitable for a specific operating point. A grey box Nonlinear Autoregressive Network was proposed in [7] that included mechanistic knowledge and empirical data. However, this technique is highly dependent on the training data and, thus far, has not been used to design controllers.

Screw extrusion cannot be utilized for ceramic processing since ceramic pastes are abrasive and will severely damage the threads, eventually causing the screw extruder to fail. Therefore, ram extrusion is used in ceramic processing. For ram extrusion, the pressure gradation and unstable shear stress regimes are much more complex. Modeling and controlling the extrusion pressure of the liquid–solid phase paste generally presents more difficulties, as compared to polymer extrusion, because of unpredictable disturbances such as air bubble release and agglomerate breakdown [8,9], material property uncertainties generated during the paste preparation procedures, and the complex variation of paste properties during extrusion due to liquid phase migration [10]. Research in the modeling and control of ram extrusion processes has not received the attention given to screw extrusion processes. A research study conducted by Mason *et al*. [11] explored the dynamic characteristics of a ram extrusion process for an aqueous–based alumina ceramic paste. The results showed that the dynamic process is well described by a first order model; however, there was tremendous variation in the time constant, which was 200–900 *sec*. Another study [12] explored the feedback control of this ram extrusion process. A bang–bang control strategy was utilized. Although good results were obtained, the strategy is not systematic and requires substantial trial and error to determine the controller parameters. Also, this control strategy was only utilized for constant extrusion force reference trajectories.

This paper proposes an adaptive controller to regulate the extrusion force in the FEF process. The rest of the paper is organized as follows. First, the experimental system and FEF process are described. Next, variation in the force extrusion model parameters is investigated experimentally. In the fourth section the adaptive extrusion force controller is designed and its

performance is analyzed. Several parts are fabricated using the proposed adaptive extrusion force controller in the final section.

Experimental System and Process Parameters and Disturbances

This section describes the machine used for the experimental studies conducted in this paper, the FEF process parameters, and the disturbances that affect the FEF process.

Hardware and Software Systems

The motion system, shown in Figure 1, consists of a gantry with three orthogonal linear axes (Velmex BiSlide), each with a 250 *mm* travel range. The X–axis consists of two parallel slides and is used as the support for the Y–axis. The Z–axis is mounted on the Y–axis and the extrusion mechanism is mounted on the Z–axis. All axes have limit switches on both ends. Four DC motors (Pacific Scientific PMA22B) drive the axes, each with a resolver for position feedback. The signal sent from the resolver is converted by a resolver–to–digital encoder converter. Each motion axis has a maximum speed of 127 *mm*/*s* and a resolution of 2.54 μm. The axes are controlled by a Delta–Tau Turbo PMAC (Programmable Multi–Axis Controller) PCI board. The axis command voltages are sent from 16 bit Digital to Analog Converters (DACs) with ranges of ±5 *V*.

The extrusion mechanism, shown in Figure 1, is a ram extruder driven by a DC motor (Kollmorgen AKM23D), which has an encoder with a resolution of 0.254 μm. The input signal to the ram axis drive is voltage from a 16 bit DAC with a range of ±5 *V*. The control signal is limited to a range of ±0.610 *V* to prevent system damage due to excessive ram speeds. A load cell (Omega LC305–1KA) is mounted between the plunger and the ram extruder to measure the

extrusion force. A 16 bit analog–to–digital conversion board (Delta–Tau ACC28) with a voltage range of ±5 V converts the analog signal from the load cell into a digital signal in the PMAC board. The force measurement resolution is 2.2 N.

The motion gantry system is housed inside a freezer. A condenser maintains the environmental temperature at $0°C$ ($\pm 2°C$). Liquid nitrogen can be used to lower the environmental temperature to $-30°C$. A temperature controller (Omega CN132) is used to control the environmental temperature by turning a solenoid valve on and off, which regulates the flow rate of liquid nitrogen. As shown in Figure 2, heating coils are installed around the material reservoir and the nozzle to keep the paste temperature at approximately 10–15°C to prevent it from freezing and ensure continuous extrusion.

Control of the motion gantry system is realized by embedded Proportional plus Integral plus Derivative controllers on the PMAC control board. Estimation and control algorithms for the extrusion mechanism are implemented in PLC programs, which are also provided by the PMAC control system, and can be programmed to implement customized algorithms. Since the PMAC control environment is originally designed for motion control, PLC programs have a lower priority than the motion controllers and are typically executed asynchronously. However, timers are used to ensure a constant sample rate. In the experiments conducted in this paper, the extrusion force control loop is executed at 10 Hz. The control system schematic is shown in Figure 3.

Process Parameters

The FEF operation process parameters include reference extrusion force, reference extrusion force derivative, deposition path offset distance, standoff distance (i.e., layer thickness), table

speed, and environmental temperature. The path offset distance and standoff distance are mainly determined by the nozzle size. Since 580 μm diameter nozzles are used for the experiments conducted in this paper, the path offset distance and standoff distance are both empirically determined to be 500 μm for proper deposition. The table speed must be matched to the extrusion force for proper part fabrication. For a given extrusion force, if the table speed is too high fully dense tracks are not formed and, if the table speed is too low, the ceramic bead is too large and covers the nozzle. The table speed is set to 10 mm/s for the experiments conducted in this paper such that operation productivity is maintained without the need for an excessive extrusion force. Environmental temperature affects the extrudate rheological properties. The environmental temperature is set to $0°C$ for the experiments conducted in this paper. See [13] for further details of the effect environmental temperature has on FEF processes.

Similar to other studies, extrusion force is selected to be the controlled variable because it directly affects the extrusion rate. The larger the extrusion force, the higher the extrusion rate, and vice versa. An experiment is performed to explore the extrusion force operating range. A constant voltage of 30 mV is sent to the ram motor amplifier and the result is shown in Figure 4. The extrusion force continuously increases until it reaches 2002 N at 219.1 sec, and then suddenly drops to 1252 N. It is observed that the paste began to come out from the top of the material reservoir due to the large extrusion force. After this occurs, the paste continuously extrudes from both the nozzle and the top of the material reservoir and the extrusion force remaines at approximately 1160 N. According to operator experience, the maximum extrusion force is set to 1558 N, which is large enough for normal operation and low enough to protect the extrusion mechanism.

Reference extrusion force derivative is another important process parameter. Typically, the initial reference extrusion force is manually selected to be between 315 and 405 *N*, depending on paste properties, which vary from batch to batch. The higher the paste apparent viscosity, the larger the initial reference extrusion force. It is necessary to continually increase the reference extrusion force during the operation to maintain a constant extrusion rate. Experiments show that the extrusion rate slowly decreases as the amount of paste in the material reservoir reduces when the extrusion force is maintained constant. Since the table speed is constant during fabrication, the decrease in extrusion rate may result in under–filling, generating discontinuous paste flow in the building area as shown in Figure 5. Nozzle clogging may even occur. It is believed that the continuous decrease of extrusion rate is related to liquid phase migration during the extrusion process [10]. The extrusion force causes a redistribution of the paste liquid and solid phases during the extrusion process, subsequently changing the paste rheological properties (typically the paste apparent viscosity will increase). When the paste is compressed, the water moves toward the die region more quickly than the paste; therefore, the water content becomes highest in the die region and decreases until it is a minimum at the top of the material reservoir. This change affects the extrusion rate. Typically, the reference extrusion force needs to be increased to maintain the desired extrusion rate [8]. The reference extrusion force derivative is selected to be $2.2 \cdot 10^{-2}$ *N*/*s*, from operator experience, for the experiments conducted in this paper.

Process Disturbances

Disturbances affecting the FEF process include liquid phase migration, agglomerate breakdown, and air bubble release. Liquid phase migration causes the paste to become drier during the operation and, thus, become more difficult to extrude, as discussed above. Regardless of how

well the paste is prepared, it will always contain agglomerates (i.e., groups of ceramic particles) and air bubbles. When the ram is applied to the paste, the agglomerates will "slide" past one another in the material reservoir, which causes the agglomerates to break into smaller agglomerates and cause fluctuations in the extrusion force. Further, based on experimental observations, a large agglomerate breakdown in the nozzle region causes the extrusion force to increase. As the air bubbles migrate towards the nozzle, they join together and, when an air bubble leaves the nozzle, the extrusion force drops. This effect is shown in Figure 6. In this experiment the periodic voltage signal sent to the ram motor drive was 21.4 *mV* for 10 s*ec*, –9.2 *mV* for 5 s*ec*, 18.3 *mV* for 15 s*ec*, and –6.1 *mV* for 5 *sec*. The extrusion force fluctuates periodically and, when an air bubble release occurs at 1836 *sec*, the extrusion force suddenly drops from 285 *N* to 55.9 *N*, and then slowly increases to the previous range.

Model Parameter Variations in FEF Processes

The FEF process contains many disturbances, as described above. Also, the paste composition is slightly different from batch to batch due to variations in the preparation, which includes material mixing and ball milling, and cannot be totally eliminated. Storage time and environmental conditions, such as temperature and humidity, also affect the paste properties. In this section Recursive Least Squares (RLS) is applied to the FEF process to estimate the dynamic model parameters for different batches of paste, and for a single reservoir of paste as it is being extruded, to analyze model parameter variations for different batches and as the amount of paste in the reservoir changes.

Alumina paste is utilized for the experiments conducted in this paper. The paste is a combination of Al_2O_3 powder, PEG, glycerol, Darvan C, and water. The materials are mixed and

then ball milled for twenty–four hours to break up agglomerates and produce a uniform mixture. Aquazol is dissolved in water at 60°*C* using magnetic stirring to form a 50 vol. % Aquazol solution. The Aquazol solution is added using a vacuum mixer (Whip Mix, Model F) to minimize bubbles. The final viscosity is adjusted by adding acid to control the paste pH.

Model Parameter Estimation

It has been shown that the ceramic paste extrusion force dynamics can be characterized as a first–order dynamic system [11]. Therefore, the extrusion force transfer function is

$$G(z) = \frac{F(z)}{u(z)} = \frac{K(1-a)}{z-a} \tag{1}$$

where z is the forward shift operator, F is the extrusion force, and u is the command voltage sent to the ram motor amplifier. The parameter K is the process gain, which is unknown. The parameter a, which is also unknown, is related to the process time constant. The difference equation corresponding to Eq. (1) is

$$F(k) = aF(k-1) + K[1-a]u(k-1) = \boldsymbol{\eta}(k-1)\boldsymbol{\varphi}(k-1) \tag{2}$$

where k is the iteration number and the unknown parameter and the regression variable vectors, respectively, are

$$\boldsymbol{\eta} = \begin{bmatrix} a & K(1-a) \end{bmatrix} = \begin{bmatrix} a & b \end{bmatrix} \tag{3}$$

$$\boldsymbol{\varphi} = \begin{bmatrix} F(k-1) & u(k-1) \end{bmatrix}^T \tag{4}$$

Parameter estimates are then computed recursively using the following equations

$$\mathbf{q}(k) = \mathbf{P}(k-1)\boldsymbol{\varphi}(k)\left[\mathbf{I} + \boldsymbol{\varphi}^T(k)\mathbf{P}(k-1)\boldsymbol{\varphi}(k)\right]^{-1} \tag{5}$$

$$\hat{\boldsymbol{\eta}}(k) = \hat{\boldsymbol{\eta}}(k-1) + \mathbf{q}(k)\left[F(k) - \boldsymbol{\varphi}^T(k)\hat{\boldsymbol{\eta}}(k-1)\right] \tag{6}$$

$$\mathbf{P}(k) = \left[\mathbf{I} - \mathbf{q}(k)\boldsymbol{\varphi}^T(k)\right]\mathbf{P}(k-1) \tag{7}$$

where $\hat{\boldsymbol{\eta}}(k)$ is the estimated parameter vector. The matrix **I** is a two–by–two identity matrix. The matrix **P** is known as the covariance matrix. The initial covariance matrix is typically selected to be a large positive definite diagonal matrix. In the experimental studies conducted in this paper, $\mathbf{P}(0) = \begin{bmatrix} 1000 & 0 \\ 0 & 1000 \end{bmatrix}$ and covariance resetting is not applied. In this form, RLS is applied to experimental data to estimate the model parameters *a* and *b*. The time constant and gain, respectively, are derived from the estimated model parameters as

$$\tau = -\frac{T}{\ln(a)} \tag{8}$$

$$K = \frac{b}{1-a} \tag{9}$$

where *T* is the sample period.

An experiment is conducted to investigate the ability of RLS to estimate FEF process model parameters. The command voltage is a periodic signal that is 24.4 *mV* for 5 *sec* and –17.1 *mV* for 5 *sec*. Positive and negative input voltages cause advancing and retreating ram motions, respectively. Note that the magnitudes of the positive and negative inputs are not equal. Since it typically requires more energy for the ram to advance than to retreat, the input magnitude in the positive direction is greater than the input magnitude in the negative direction in an attempt to maintain a constant average extrusion force. By using Eqs. (5)–(7) and initial model parameters of $\hat{a}(0) = 0.8$ and $\hat{b}(0) = 0.4$, the model parameters are estimated. The modeled and measured extrusion force, as well as the model parameter estimates, are shown in Figure 7 for the entire operation. The modeled extrusion force matches the measured extrusion force very well with an average percent error of 2.4% and a maximum percent error of 8.4%. The model parameter

estimates during the steady state are shown in Figure 8. The settling time for the model parameter estimates is 3.2 *sec*, which is very quick as compared to build times that can vary between several minutes to a few hours. This experiment indicates that RLS can be applied to estimate extrusion force model parameters for the FEF process.

Model Variation Analysis

As previously mentioned, paste compositions are slightly different from batch to batch. A similar phenomenon was also reported by Costin *et al*. [5]. To investigate the effect paste batch preparation has on the force extrusion model parameters, model parameters for four reservoirs of paste, each from a different batch, are estimated. Each experiment starts with a reservoir of unused paste with an initial volume of approximately 40 *ml*. The command voltage periodically changes between constant values of –3.7 and 8.5 *mV* every 5 *sec*. The time constants and gains are calculated using Eqs. (5)–(9). Each experiment is conducted for 120 *sec* and the average time constants and gains are shown in Table 1. It can be seen that both model parameters are very different for the four batches of paste. The range of the estimated time constants divided by the mean of the time constants is 0.52 and the range of the estimated gains divided by the mean of the gains is 0.65.

Even for the same batch of paste, the paste properties for different reservoirs of paste will be different because of variations in storage time, temperature, humidity, etc. Moreover, for the same tube of paste, the paste properties will also change during the extrusion process, as reported in [10]. Experiments are conducted to investigate how the extrusion dynamic model parameters vary during the FEF process as the amount of paste in the material reservoir decreases. In these experiments, a reservoir of paste with an initial volume of approximately 35 *ml* is extruded. The

command voltage changes periodically and is 12.2 *mV* for 10 *sec*, –6.1 *mV* for 5 *sec*, 6.1 *mV* for 10 *sec*, and 0 *mV* for 5 *sec* for each experiment, and approximately 5 *ml* of paste is extruded over a period of approximately 2000 *sec*. Average time constants and gains (shown in Figure 9) are calculated from the last 100 *sec* of data collected for each experiment.

Figure 9 shows that as the volume of paste in the material reservoir decreases the time constant decreases and the gain increases. It is hypothesized that the changes in the time constant and gain as paste is extruded are associated with changes in the paste rheological properties. As paste is extruded, liquid phase migration causes the paste to become drier and the number of air bubbles decreases as they are released. Both phenomena cause the paste to become stiffer and more viscous; therefore, the time constant decreases and less time is required for the extrusion force to reach the steady state. Also, as the paste becomes less elastic and more viscous, it is harder to compress, and the gain increases.

These experiments demonstrate that different batches of paste have much different extrusion force dynamic properties and, even for the same reservoir of paste, the extrusion force dynamic properties change substantially as the amount of material in the reservoir decreases. Therefore, an adaptive control scheme is adopted in this paper to account for the inherent model parameter variations by updating the controller gain calculated from the model parameters in real time.

Adaptive Extrusion Force Controller

An adaptive general tracking controller used to regulate the extrusion force in FEF processes is designed and discussed in this section.

Tracking Controller Design

The extrusion force model is

$$F(k) = aF(k-1) + bu(k-1) \tag{10}$$

The error is

$$e(k) = F_r(k) - F(k) \tag{11}$$

where F_r is the reference extrusion force. Substituting Eq. (11) into Eq. (10)

$$e(k) = F_r(k) - aF(k-1) - bu(k-1) \tag{12}$$

Noting that $e(k–1) = F_r(k–1) – F(k–1)$, solving for $F(k–1)$, and substituting this expression into Eq. (12)

$$e(k) = ae(k-1) + F_r(k) - aF_r(k-1) - bu(k-1) \tag{13}$$

Defining the pseudo control signal $\mu(k–1) = F_r(k) – aF_r(k–1) – bu(k–1)$, Eq. (13) can be rewritten as

$$e(k) = ae(k-1) + \mu(k-1) \tag{14}$$

A controller of the form $\mu(k–1) = ge(k–1)$ is used where the controller gain g is adjusted to shape the error transient response. In the adaptive control scheme, the model parameters a and b are estimated in real time and the controller gain g is updated in real time given the estimated value of a

$$g = \exp\left(-\frac{T}{\tau_d}\right) - \hat{a} \tag{15}$$

where τ_d is the desired closed–loop time constant. The physical control signal is

$$u(k-1) = \frac{F_r(k) - \hat{a}F_r(k-1) - ge(k-1)}{\hat{b}} \tag{16}$$

Note that this controller requires future knowledge of the reference signal, which is typically available. The controller is able to intelligently modify its gain to maintain stability and a consistent transient response as the extrusion force process varies. Also, when different batches of paste and reservoirs of material are used, the adaptive controller quickly estimates the model parameters and adjusts its gain.

General Tracking Controller Implementation

The general tracking controller is implemented in PLC programs of the Turbo PMAC control system. The control law is proved (see Appendix) to be able to achieve a unitary closed–loop transfer function, assuming zero initial conditions. Therefore, theoretically, this controller extends the tracking bandwidth to infinity. Practically, the system tracking bandwidth is limited due to unmodeled dynamics, sample rate, control signal magnitude limitation, disturbances, etc. The sample rate is 10 *Hz*, which is more than sufficient for the extrusion process since the smallest time constant is approximately 61.4 *sec*, as shown in Figure 9. To investigate controller performance, experiments with three different reference signals (i.e., sinusoidal, triangular, and square) are conducted. The closed–loop time constant is selected to be 0.1 *sec* to achieve the fastest response possible given the sample rate limitation. All experiments are conducted using the same batch of alumina paste.

Sinusoidal Reference

Sinusoidal reference extrusion forces with frequencies ranging from 0.1 to 1 *Hz* and peak–to–peak amplitudes of 89 *N* are utilized in the first set of experiments. Figure 10 shows the extrusion force and control signal responses for a reference with a frequency of 0.1 *Hz*. It can be seen that

there are some fluctuations in the extrusion force. These fluctuations are caused by process effects, such as agglomerate breakdown, and motor commutation effects. During the steady–state, the control signal is very small, usually between –50 and 50 *mV*; therefore, the ram motor rotates at a very low speed and motor commutation causes fluctuations in the ram velocity, which causes fluctuations in the extrusion force. Figure 11 shows the extrusion force and control signal responses for a reference with a frequency of 1 *Hz*. The controller sample rate is 10 *Hz*; therefore, there are 10 samples/cycle for the reference with a frequency of 1 *Hz*, which is much less than the 100 samples/cycle for the reference with a frequency of 0.1 *Hz*. Therefore, the fluctuations in the measured force signals are significantly reduced and, subsequently, the fluctuations in the control signals are much less. Since more control effort is required to track the reference with the higher frequency, the control signal is larger and is between –500 and 500 *mV*.

The data is used to create magnitude and phase frequency plots of the closed–loop system, as shown in Figure 12. The magnitude is between –0.05 and 0.21 *dB* and tends to decrease as the frequency increases. This is within six resolutions of the force sensor. The phase is zero for low frequencies, decreases as the frequency increases, and is a minimum of –9.8° at a frequency of 1 *Hz*. Figure 13 shows the average absolute value of the extrusion force error and the standard deviation of the absolute value of the error. The average absolute value of the error increases as the frequency increases and is a maximum of 10.6 *N*, which is within five resolutions of the force sensor. The standard deviation increases as the frequency increases and is a maximum of 7.79 *N*, which is within four resolutions of the force sensor.

Triangular Reference

Triangular extrusion force references with frequencies ranging from 0.1 to 1 *Hz* and peak–to–peak amplitudes of 89 *N* are utilized in these experiments. Figure 14 shows the extrusion force and control signal responses for a reference with a frequency of 0.1 *Hz*. Figure 15 shows the extrusion force response for the reference with a frequency of 1 *Hz*. As more control effort is used to perform the higher frequency tracking, the control signals are between –250 to 200 *mV*, larger than the control signals in Figure 14. The tracking performance is very good in both experiments. Again, there are fluctuations in the extrusion force due to process and motor commutation effects.

The data is used to create magnitude and phase frequency plots of the closed–loop system, as shown in Figure 12. The magnitude is between –0.301 and 0.051 *dB* and tends to decrease as the frequency increases. This is within six resolutions of the force sensor. The phase is zero for low frequencies, decreases as the frequency increases, and is a minimum of –11.9° at a frequency of 1 *Hz*. Figure 13 shows the average absolute value of the extrusion force error and the standard deviation of the absolute value of the error. The average absolute value of the error increases as the frequency increases and is a maximum of 9.08 *N*, which is within five resolutions of the force sensor. The standard deviation increases as the frequency increases and is a maximum of 6.03 *N*, which is within three resolutions of the force sensor.

Square Reference

Square reference extrusion forces with frequencies ranging from 0.1 to 1 *Hz* and peak–to–peak amplitudes of 89 *N* are utilized in this set of experiments. Figure 16 shows the extrusion force and control signal responses for a reference with a frequency of 0.1 *Hz*. It can be seen that the

control signal saturates at –610 and 610 *mV* for approximately 0.09 *sec* when the reference signal decreases and increases, respectively. However, the steady–state control signal is between –30 and 30 *mV*. Figure 17 shows the extrusion force and control signal responses for a reference with a frequency of 1 *Hz*. As the reference changes values, the control signal saturates between –610 to 610 *mV* for about 0.09 *sec*, similar to Figure 16. The settling time is approximately 0.1–0.2 *sec* for both experiments. This is three orders of magnitude less than the open–loop settling time, which is in the range of 246 to 736 *sec*.

The data is used to create magnitude and phase frequency plots of the closed–loop system, as shown in Figure 12. The magnitude is between –0.115 and 0.204 *dB* and tends to decrease as the frequency increases. This is within four resolutions of the force sensor. The phase is –0.15° for low frequencies, decreases as the frequency increases, and is a minimum of –15.1° at a frequency of 1 *Hz*. Figure 13 shows the average absolute value of the extrusion force error and the standard deviation of the absolute value of the error. The average absolute value of the error increases as the frequency increases and is a maximum of 13.1 *N*, which is within six resolutions of the force sensor. The standard deviation increases as the frequency increases and is a maximum of 21.5 *N*, which is within ten resolutions of the force sensor. The errors, and standard deviations of the errors, are larger for the experiments with square references than the experiments with sinusoidal and triangular references since the control signal saturated in the experiments with square references.

Part Fabrication

Three ceramic parts are fabricated using the proposed control scheme presented above. The first part is an ogive cone with a 25.4 *mm* diameter base and a 50.8 *mm* height. The part is fabricated

without the controller using a constant ram velocity of 10 $\mu m/s$. A photograph of the part is shown in Figure 18 and the corresponding extrusion force time history is shown in Figure 19. Without extrusion force control the part fabrication fails. The extrusion force varies significantly, leading to inconsistent material deposition and, eventually, part collapse. The part is also fabricated using the extrusion force controller. A photograph of the part is shown in Figure 20 and the corresponding extrusion force and command voltage time histories are shown in Figure 21. In this case, the extrusion force followed the reference extrusion force very well and the part was successfully fabricated. The mean absolute value of the extrusion force error is 3.57 *N*, which is within two sensor resolutions, and the maximum absolute value of the extrusion force error is 14.6 *N*, which is within seven sensor resolutions. The extrusion force variations seen in this experiment are again due to process effects such as agglomerate breakdown and the fact that the motor is operating at very low speeds. This example illustrates the need for intelligent extrusion force control.

The second part is a large ogive cone with a 50.8 *mm* diameter base and a 152.4 *mm* height that is fabricated using the extrusion force controller. This part requires nearly an entire reservoir of paste. A photograph of the part is shown in Figure 22 and the corresponding extrusion force and command voltage time histories are shown in Figure 23. Again, the extrusion force tracked the reference extrusion force very well. The mean absolute value of the extrusion force error is 1.83 *N*, which is within one sensor resolution, and the maximum absolute value of the extrusion force error is 8.22 *N*, which is within four sensor resolutions. Again, the extrusion force variation is not constant throughout the experiment. This example illustrates the ability of the controller to regulate the extrusion force even as the process changes due to large changes in the amount of paste in the material reservoir.

In the next experiment two square parts, 38.1 *mm* along each side, are fabricated. The first part is fabricated using the extrusion force controller and a constant reference extrusion force of 311 *N*. Since the time duration to fabricate these parts is so short, the reference extrusion force derivative was zero. A photograph of the part is shown in Figure 24 and the extrusion force and command voltage time histories are shown in Figure 25. The extrusion force tracked the reference value very well. The mean absolute value of the extrusion force error is 1.02 *N*, which is within one sensor resolution, and the maximum absolute value of the extrusion force error is 5.05 *N*, which is within three sensor resolutions. However, the part quality is visually poor, particularly at the corners. This is due to the fact that the motion axes are accelerating and decelerating at these locations, causing excessive material deposition.

The second square is also fabricated using the extrusion force controller; however, reference extrusion force varies. The reference extrusion force is 311 *N* during the straight sections, but is ramped down to 89 *N* at the corners. A photograph of the part is shown in Figure 26 and the corresponding extrusion force and command voltage time histories are shown in Figure 27. The extrusion force tracked the reference value very well. The mean absolute value of the extrusion force error is 15.0 *N* and the maximum absolute value of the extrusion force error is 192 *N*. The large errors in the extrusion force are due to the sharp changes in the reference extrusion force at the part corners. The reference force rate of change causes the controller to saturate during these periods and large errors to occur. This is seen in Figure 27. The part quality of the square fabricated using a variable reference extrusion force is visually much better, even at the corners, than the square fabricated using a constant extrusion reference force. This is due to variable reference extrusion force, which decreases sharply at the corners. This causes the extrusion force to decrease and, thus, less material is extruded while the motion axes are

accelerating and decelerating. This, in turn, causes the material deposition per unit length to be constant. Note that the reference extrusion force trajectory is determined empirically. If a process model were available, this trajectory could be computed analytically.

Summary and Conclusions

Recursive Least Squares (RLS) was applied to estimate the parameters of a first–order dynamic model of the Freeze–form Extrusion Fabrication process in real time. An adaptive controller with a general tracking control law was designed and implemented to regulate the extrusion force. Experiments with sinusoidal, triangular, and square extrusion force references with different frequencies ranging from 0.1 to 1 *Hz* were conducted to investigate the controller's performance. Several parts were also fabricated using the proposed extrusion force controller.

The experimental results show that the model parameters are not only different from batch to batch, but also change significantly during the extrusion process. It is observed that the time constant decreases and the gain increases as the paste in the material reservoir decreases. The reason for these trends is believed to be related to liquid phase migration. The adaptive controller demonstrated excellent tracking for all reference force trajectories over a wide range of frequencies. The adaptive controller provides an automated means to determine the controller parameters when a new batch of paste is utilized and can adjust the controller parameters automatically during the extrusion process to account for disturbances and inherent changes in the process due to liquid phase migration. The part fabrication studies illustrated the need for extrusion force control and the excellent performance of the proposed adaptive extrusion force controller. When the motion system axes accelerate or decelerate, as was the case for the square parts, geometric integrity is sacrificed when using a constant extrusion force. A variable

reference force trajectory, which can be robustly tracked by the proposed control strategy, provides improved part geometry. In this paper the reference force was empirically determined. Future studies will seek to develop a process model that will be used to construct the reference extrusion force trajectory when the motion system axes accelerate or decelerate.

Acknowledgements

The authors wish to acknowledge the financial support for this work from the Missouri University of Science and Technology's Center for Aerospace Manufacturing Technologies (Air Force Research Laboratory contract FA8650–04–C–5704) and the technical support of colleagues at Missouri S&T (especially Mike Mason, Tieshu Huang and Greg Hilmas), the Boeing Company (especially Mike Hayes and Sam Easley), and the Air Force Research Laboratory.

References

1. Lous, G.M., Cornejo, I.A., McNulty, T.F., Safari, A., and Danforth, S.C., 2000, "Fabrication of Piezoelectric Ceramic/Polymer Composite Transducers using Fused Deposition of Ceramics," *Journal of the American Ceramic Society,* **83**(1), pp. 124–128.
2. Huang, T.S., 2007, "Fabrication of Ceramic Components Using Freeze–form Extrusion Fabrication," Ph.D. Dissertation, Department of Materials Science and Engineering, University of Missouri–Rolla, Rolla, Missouri.
3. Costin, M.H., Taylor, P.A., and Wright, J.D., 1982, "A Critical Review of Dynamic Modeling and Control of Plasticating Extruders," *Polymer Engineering and Science*, **22**(7), pp. 393–401.

4. Hassan, G.A. and Parnaby, J., 1981, "Model Reference Optimal Steady–State Adaptive Computer Control of Plastics Extrusion Processes," *Polymer Engineering and Science*, **21**(5), pp. 276–284.
5. Costin, M.H., Taylor, P.A., and Wright, J.D., 1982, "On the Dynamics and Control of a Plasticating Extruder," *Polymer Engineering and Science*, **22**(17), pp. 1095–1106.
6. Previdi, F., Savaresi, S.M., and Panarotto, A., 2006, "Design of a Feedback Control System for Real–Time Control of Flow in a Single–Screw Extruder," *Control Engineering Practice*, **14**(9), pp. 1111–1121.
7. McAfee, M. and Thompson, S., 2007, "A Novel Approach to Dynamic Modeling of Polymer Extrusion for Improved Process Control," *Proceedings of the Institution of Mechanical Engineers, Part I: Journal of Systems and Control Engineering*, **221**(4), pp. 617–628.
8. Amarasinghe, A.D.U.S. and Wilson, D.I., 1998, "Interpretation of Paste Extrusion Data," *Chemical Engineering Research and Design*, **76**(A1), pp. 3–8.
9. Russell, B.D., Wilson, D.I., Lasenby, J., and Blackburn, S., 2002, "On–Line Monitoring of Pastes Undergoing Extrusion," *Proceedings of the 4th World Congress on Particle Technology*, Sydney, Australia, July 21–25.
10. Burbidge, A.S., Bridgewater, J., and Saracevic, Z., 1995, "Liquid Migration in Paste Extrusion," *Chemical Engineering Research and Design*, **73**(7), pp. 810–816.
11. Mason, M.S., Huang, T.S., Landers, R.G., Leu, M.C., and Hilmas, G.E., 2006, "Freeform Extrusion of High Solids Loading Ceramic Slurries, Part I: Extrusion Process Modeling," *Seventeenth Annual Solid Freeform Fabrication Symposium*, Austin, Texas, August 14–16.

12. Mason, M.S., Huang, T.S., Landers, R.G., Leu, M.C., and Hilmas, G.E., 2006, "Freeform Extrusion of High Solids Loading Ceramic Slurries, Part II: Extrusion Process Control," *Seventeenth Annual Solid Freeform Fabrication Symposium*, Austin, Texas, August 14–16.

13. Zhao, X.Y., Mason, M.S., Huang, T.S., Leu, M.C., Landers, R.G., Hilmas, G.E., Easley, S.J. and Hayes, M.W., 2007, "Experimental Investigation of Effect of Environment Temperature on Freeze–form Extrusion Fabrication," *Eighteenth Annual Solid Freeform Fabrication Symposium*, Austin, Texas, August 6–8.

Appendix

The proposed controller's ability to achieve a unitary transfer function is proved in this appendix.

Taking the *z*–transform of Eq. (16) and assuming no model parameter estimation error

$$bu(z) = F_r(z)z - aF_r(z) - ge(z) \tag{A1}$$

Taking the *z*–transform of the error given in Eq. (11)

$$e(z) = F_r(z) - F(z) \tag{A2}$$

Substituting Eq. (A2) into Eq. (A1) and rearranging

$$bu(z) = [z - a - g]F_r(z) + gF(z) \tag{A3}$$

Taking the *z*–transform of Eq. (10)

$$F(z) = aF(z)z^{-1} + bu(z)z^{-1} \tag{A4}$$

Substituting Eq. (A3) into Eq. (A4) and rearranging

$$\left[1 - az^{-1} - gz^{-1}\right]F(z) = \left[1 - az^{-1} - gz^{-1}\right]F_r(z) \tag{A5}$$

Therefore, the closed–loop transfer function is

$$\frac{F(z)}{F_r(z)} = \frac{1 - az^{-1} - gz^{-1}}{1 - az^{-1} - gz^{-1}} = 1 \tag{A6}$$

Nomenclature

a,b	–	extrusion force model parameters
$\hat{a},\hat{b}$	–	estimated extrusion force model parameters
e	–	extrusion force error (N)
F	–	extrusion force (N)
F_r	–	reference extrusion force (N)
g	–	controller gain (mV/N)
G	–	extrusion force model transfer function
$\mathbf{I}$	–	2×2 identity matrix
k	–	iteration
K	–	extrusion force model gain (N/mV)
$\mathbf{P}$	–	covariance matrix
T	–	sample period (sec)
u	–	command voltage (mV)
z	–	forward shift operator
$\boldsymbol{\eta}$	–	vector of extrusion force model parameter estimates
μ	–	pseudo control signal
τ	–	extrusion force model time constant (sec)
τ_d	–	desired extrusion force time constant (sec)
$\boldsymbol{\varphi}$	–	vector of regression variables

Table 1: Estimated model time constants and gains for different batches of paste.

Batch	Time constant (*sec*)	Gain (*N/mV*)
1	108	761
2	184	410
3	125	825
4	164	550

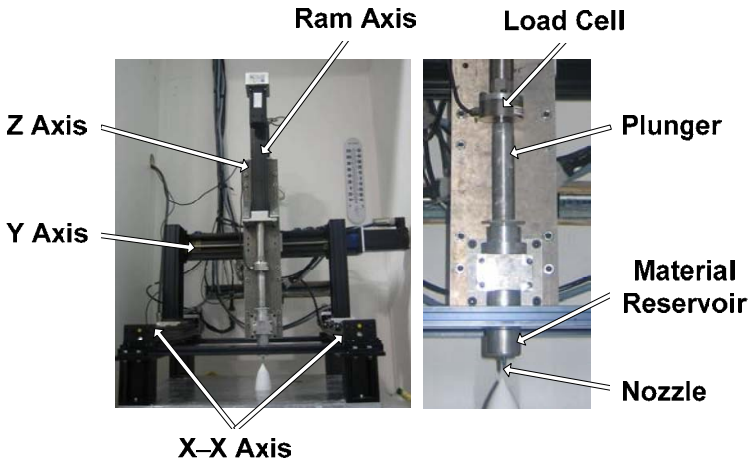

Figure 1: **Gantry motion system (left) and extrusion mechanism (right).**

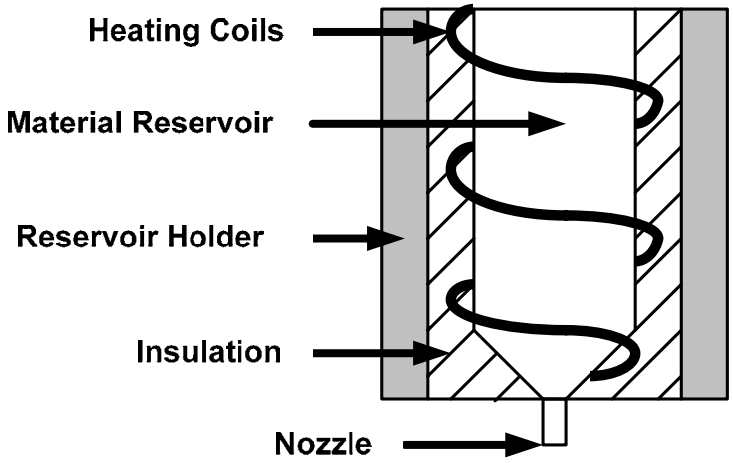

Figure 2: Extrusion mechanism schematic.

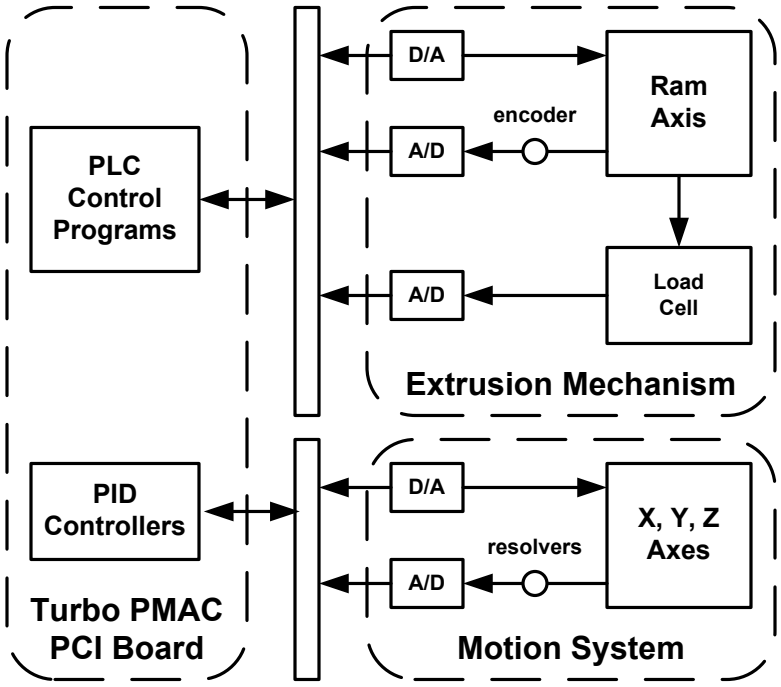

Figure 3: FEF process control system schematic.

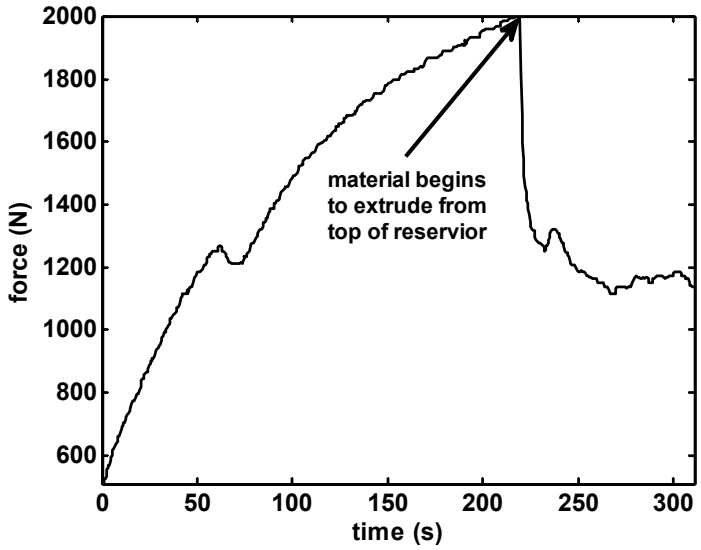

Figure 4: Extrusion force response to a constant command voltage of 30 *mV*.

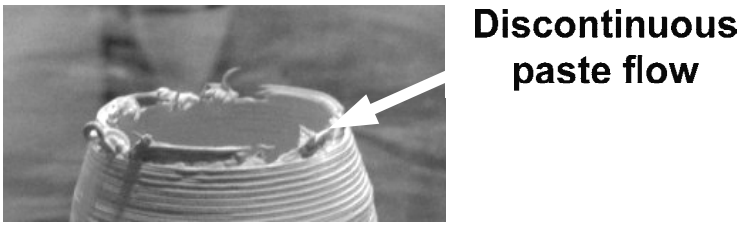

Figure 5: Discontinuous paste flow on top of a hollow cone.

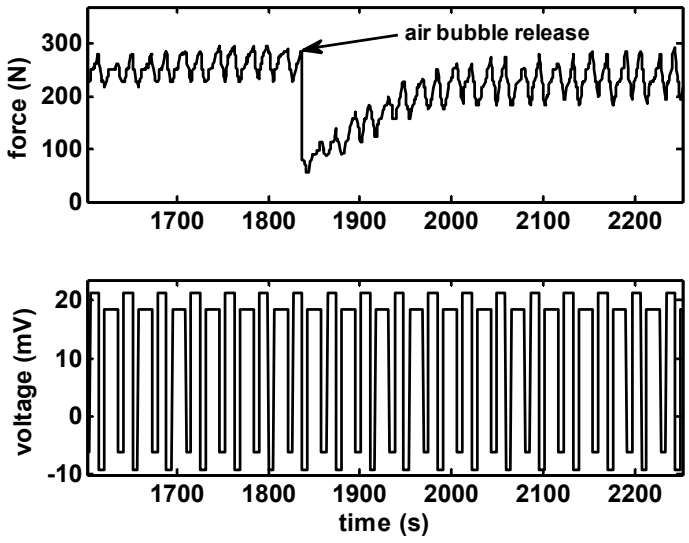

Figure 6: Extrusion force (top) and command voltage (bottom). Sudden drop in extrusion force is due to the release of an air bubble.

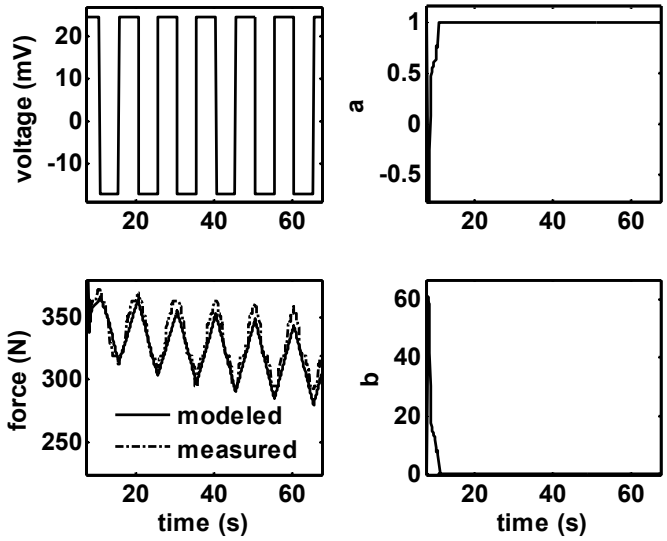

Figure 7: Commanded voltage (upper left), modeled and measured extrusion forces (bottom left), and estimated model parameters *a* (upper right) and *b* (lower right).

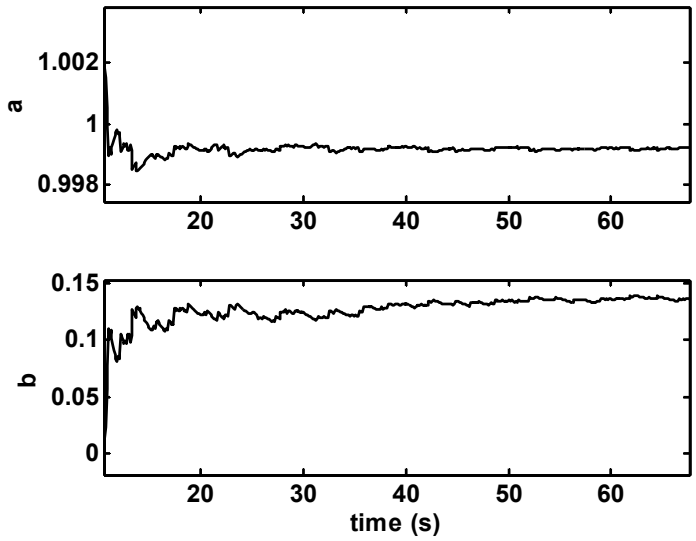

Figure 8: Estimated model parameters *a* (top) and *b* (bottom) during steady–state for experiment in Figure 7.

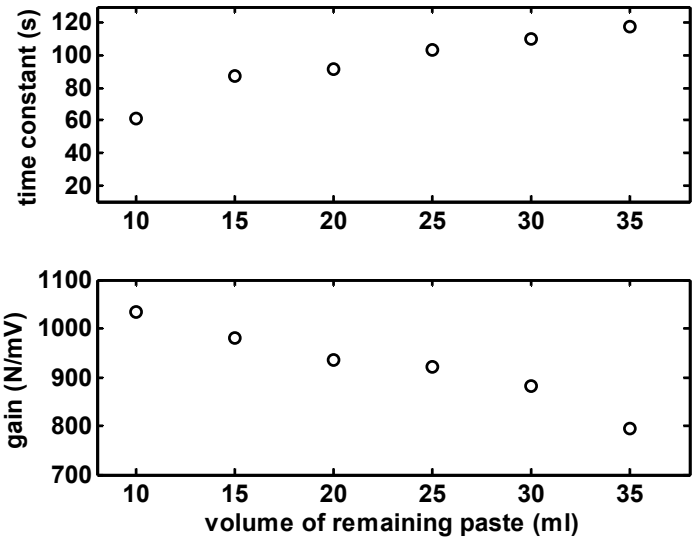

Figure 9: Model time constant (top) and model gain (bottom) as functions of paste volume in material reservoir.

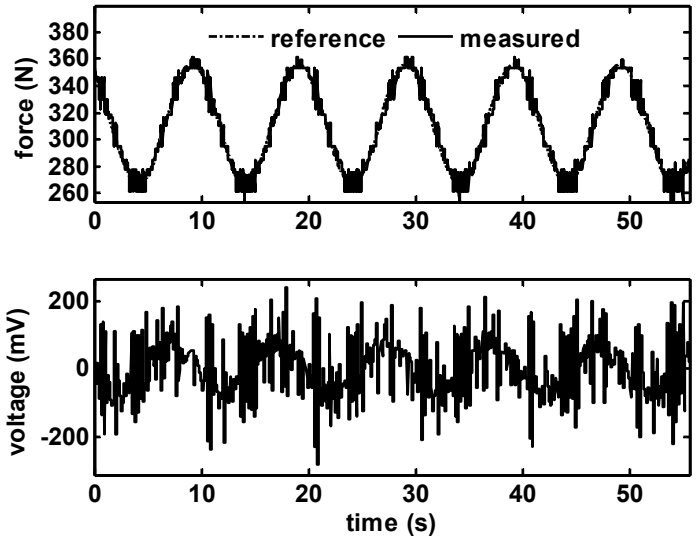

Figure 10: Reference and measured extrusion force (top) and command voltage (bottom) responses for a sinusoidal reference with a frequency of 0.1 *Hz*. The reference and measured extrusion force signals are hardly distinguishable.

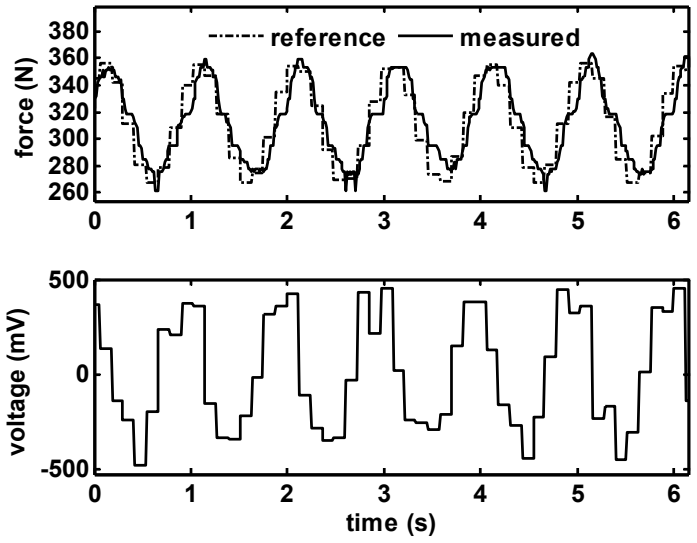

Figure 11: Reference and measured extrusion force (top) and command voltage (bottom) responses for a sinusoidal reference with a frequency of 1 *Hz*.

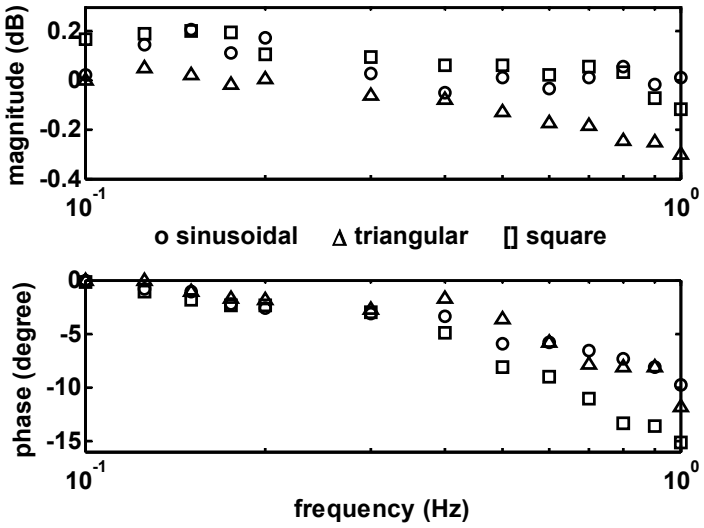

Figure 12: Experimental extrusion force closed–loop magnitude (top) and phase (bottom) frequency responses for sinusoidal, triangular, and square reference extrusion forces.

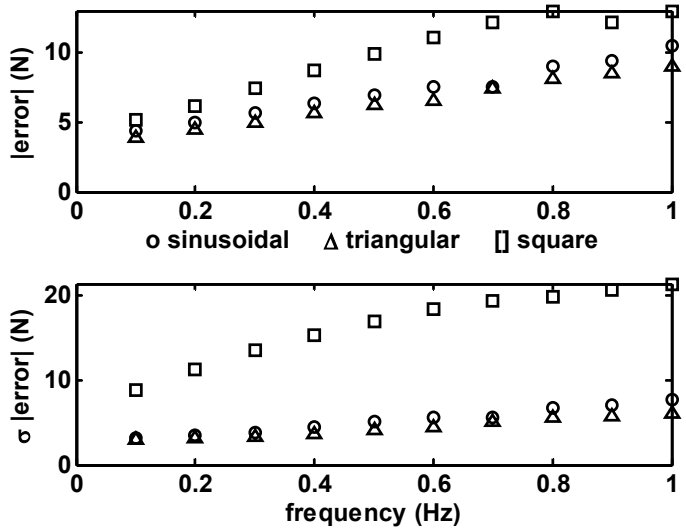

Figure 13: Extrusion force average error (top) and error standard deviation (bottom) for sinusoidal, triangular, and square reference extrusion forces.

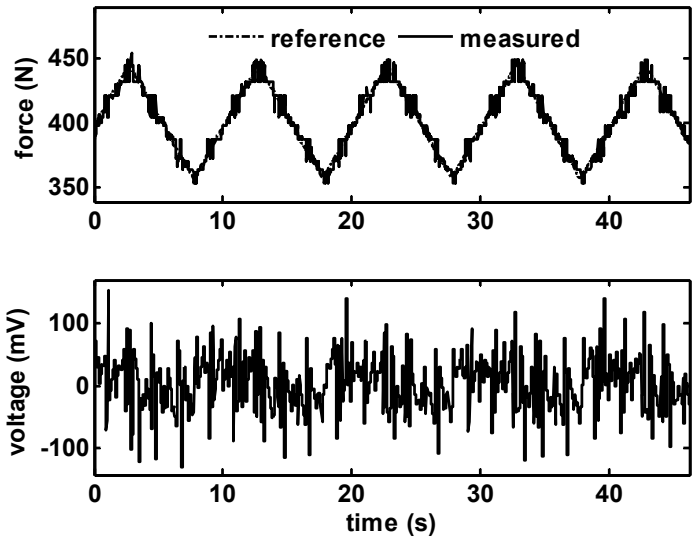

Figure 14: Reference and measured extrusion force (top) and command voltage (bottom) responses for a triangular reference with a frequency of 0.1 *Hz*. The reference and measured extrusion force signals are hardly distinguishable.

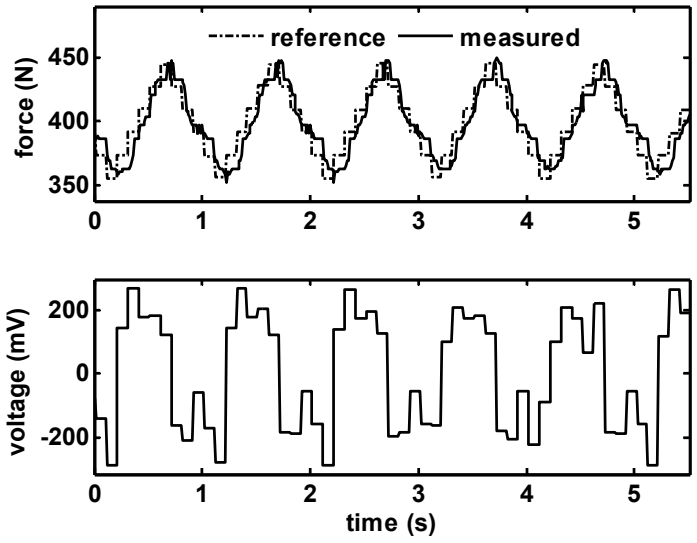

Figure 15: Reference and measured extrusion force (top) and command voltage (bottom) responses for a triangular reference with a frequency of 1 *Hz*.

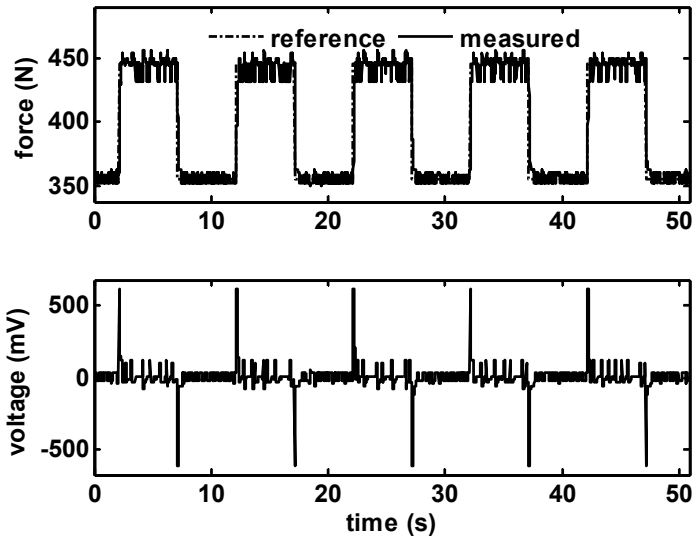

Figure 16: Reference and measured extrusion force (top) and command voltage (bottom) responses for a square reference with a frequency of 0.1 *Hz*. The reference and measured extrusion force signals are hardly distinguishable.

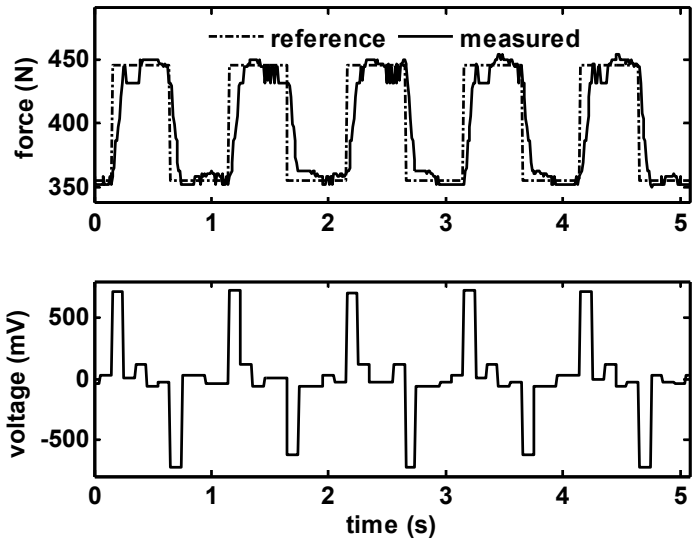

Figure 17: Reference and measured extrusion force (top) and command voltage (bottom) responses for a square reference with a frequency of 1 *Hz*.

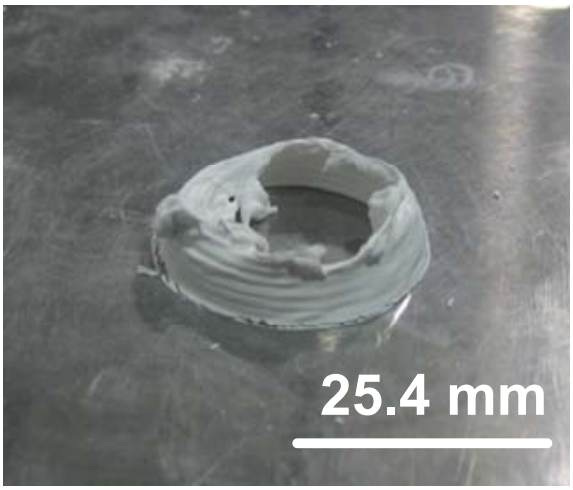

Figure 18: Small ogive cone fabricated with a constant ram velocity of 10 *μm*/*s*.

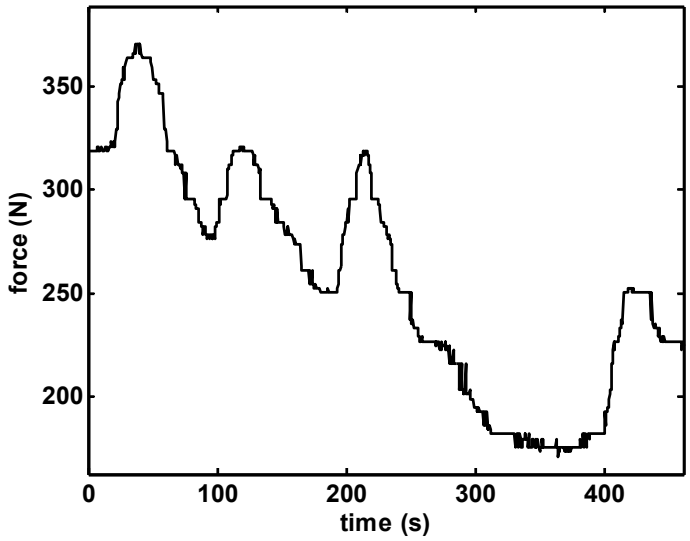

Figure 19: Extrusion force for part in Figure 18 fabricated with a constant ram velocity of 10 *μm*/*s*.

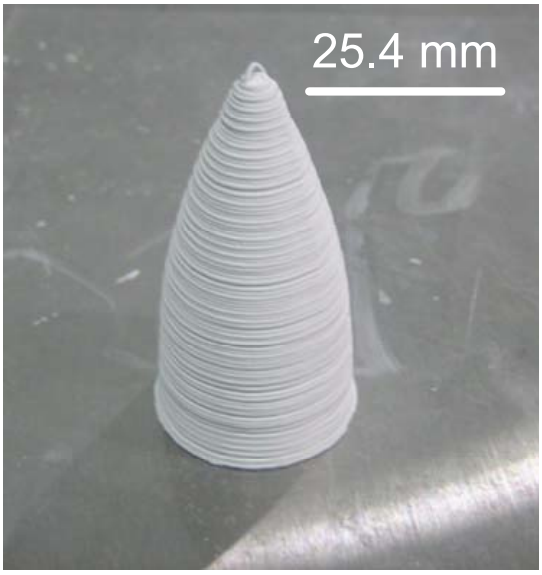

Figure 20: Small ogive cone fabricated with extrusion force controller.

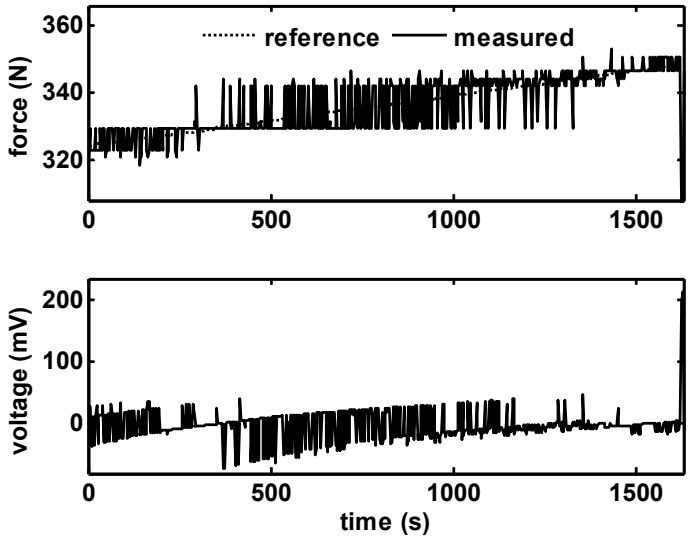

Figure 21: Extrusion force (top) and command voltage (bottom) for part in Figure 20 fabricated with extrusion force controller. The reference and measured extrusion force signals are hardly distinguishable.

Figure 22: Large ogive cone fabricated with extrusion force controller.

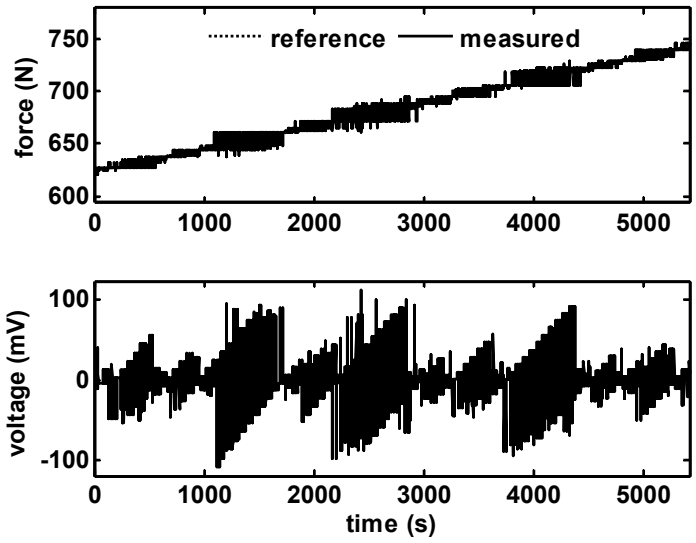

Figure 23: Extrusion force (top) and command voltage (bottom) for part in Figure 22 fabricated with extrusion force controller. The reference and measured extrusion force signals are hardly distinguishable.

Figure 24: Square part fabricated with extrusion force controller and a constant reference force of $F_r = 311\ N$.

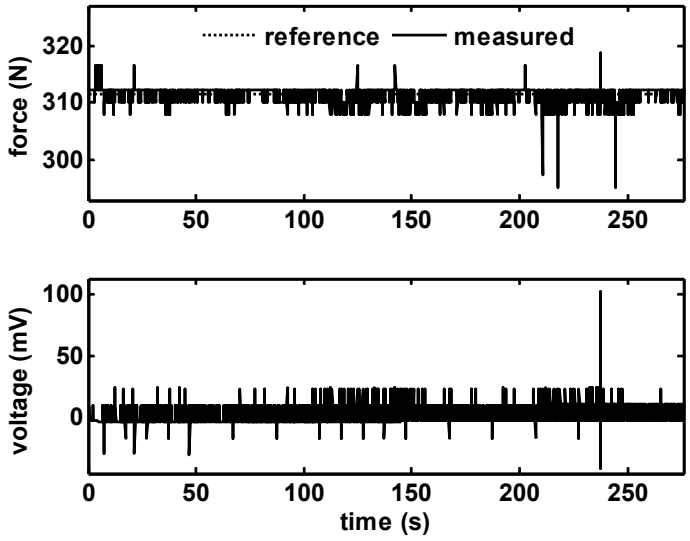

Figure 25: Reference and measured extrusion force (top) and command voltage (bottom) for square part in Figure 24 fabricated with extrusion force controller and a constant reference force of $F_r = 312\ N$. The reference and measured extrusion force signals are hardly distinguishable.

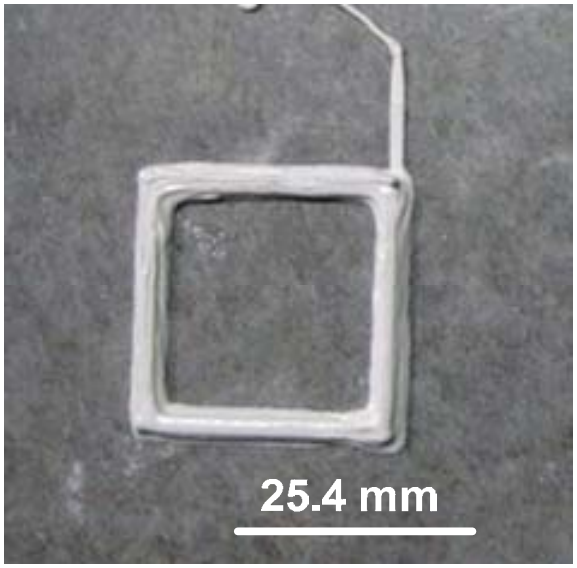

Figure 26: Square part fabricated with extrusion force controller and a variable reference force.

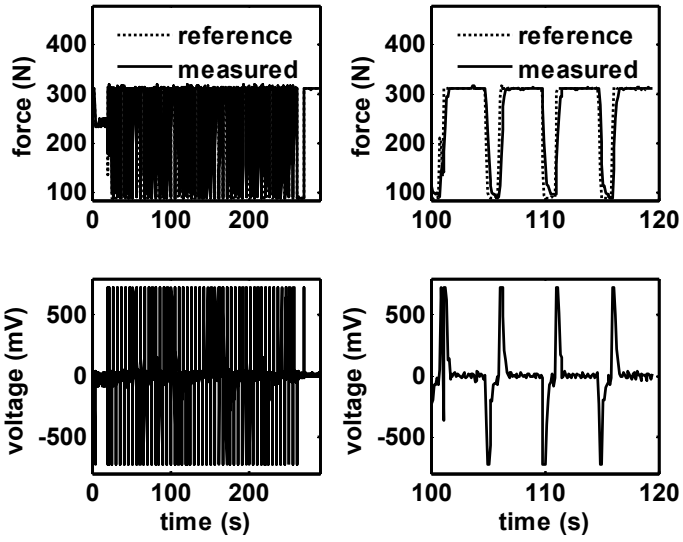

Figure 27: Reference and measured extrusion force (top) and command voltage (bottom) for square part in Figure 26 fabricated with extrusion force controller and a variable reference force.